Electronic Supplementary Material (ESI) for Journal of Materials Chemistry A.

Supporting Information

Title: Highly active and durable double-doped bismuth oxide-based oxygen electrodes for reversible solid oxide cells at reduced temperatures

Byung-Hyun Yun,[a,†] Kyeong Joon Kim,[a,†] Dong Woo Joh,[a,†] Munseok S. Chae,[a]
Jong Jun Lee,[a] Dae-won Kim,[a,b] Seokbeom Kang,[a,b] Doyoung Choi,[a,b] Seung-Tae Hong[a]
and Kang Taek Lee[a,*]

[a]*Department of Energy Science and Engineering, DGIST, Daegu 42988, Republic of Korea*
[b]*School of Undergraduate Studies, DGIST, Daegu 42988, Republic of Korea*

[†]*These authors are equally contributed to this work*

* Corresponding Author: Prof. Kang Taek Lee

Contents :

Experimental Section

Table S1-S2

Figure S1-S8

References

Experimental Section

Materials synthesis**:** $Dy_{0.08}Y_{0.04}Bi_{0.88}O_{1.5}$ (DYSB) powders were prepared using the solid state reaction method. A mixture of the desired stoichiometric amount of Bi_2O_3 (99.99% pure, YeeYoung Cerachem), Dy_2O_3 (99.99% pure, Alfa Aesar) and Y_2O_3 (99.99% pure, Alfa Aesar) was ball-milled for 24 h with the zirconia balls in the a high-density polyethylene (HDPE) bottle. The mixtures were calcined at 800 ^{o}C for 16 h. The calcined powders were finely ground using a mortar and pestle and then sieved using a 45-μm mesh. The powders were, then, uniaxially pressed at 50 MPa to obtain disk-shaped pellets, with a diameter of 10 mm, followed by sintering at 890 ^{o}C for 16 h to prepare dense pellets for electrical conductivity measurement.

Symmetrical cells preparation**:** For fabrication of symmetric cells, cathode paste was prepared by mixing DYSB and the $La_{0.8}Sr_{0.2}MnO_3$ (LSM) powders (Fuelcellmaterials) at a 50:50 (DYSB:LSM) volume ratio with a texanol-based vehicle (441 ESL Electroscience). For comparison, $Er_{0.2}Bi_{0.8}O_{1.5}$ (ESB) powders were synthesized using exactly the same solid state reaction process as that previously described and mixed with the LSM powders (Fuelcellmaterials) to fabricate the LSM-ESB cathode. The prepared cathode pastes were then brush-painted onto both sides of YSZ (Tosoh) electrolytes, followed by heat-treatment at 800 ^{o}C for 2 h to burn off the vehicle and sinter the cathodes.

Anode-supported single cell preparation**:** The Ni-YSZ anode supported cells were prepared using a tape-casting technique consisting of the following layers: Ni-YSZ anode support, Ni-YSZ anode functional layer, and YSZ electrolyte. The tape-cast half-cell layers were laminated at 100 ^{o}C via a roll calendaring process and pre-sintered stepwise to burn the organic binder system, followed by sintering at 1400 ^{o}C for 3h. The LSM-DYSB and LSM-ESB cathode pastes were screen printed on the YSZ electrolyte of the half-cells and sintered at 750 °C for 2h. To fabricate the reference LSCF-GDC cathode cell, the GDC (Rhodia) buffer layer was deposited on the YSZ electrolyte using the screen printing method and sintered at 1250 °C for 5h. The LSCF-GDC cathode prepared by ball milling the LSCF (Fuelcellmaterials) and GDC (Rhodia) powders at a 50:50 vol% was screen-printed on the GDC buffer layer and then sintered at 1050 °C for 3 h.

Characterization: Powder XRD data were collected at room temperature using an X-ray diffractometer (Rigaku Miniflex 600) with a Cu X-ray tube ($\lambda = 1.5418$ Å), secondary graphite (002) monochromator, and an angular range of $20° \leq 2\theta \leq 120°$. Crystal structures for DYSB were refined using the powder profile refinement program GSAS, in which the initial structural models of δ-Bi_2O_3 were adopted from previous neutron studies.[1, 2] TEM (Hitachi, HF-3300) was utilized at an accelerating voltage of 300 kV for analyzing the powder morphology and crystallinity. DTA was performed using a Rigaku Thermo plus EVO TG-8120. Approximately 25 mg of powder specimen in an Al_2O_3 holder was subjected to a 10 °C/min of heating and cooling cycle under 250 mL/min of air flow rate to reach 750 °C.

The electrical conductivity, electrode polarization resistance of symmetric cells, and performance of a single cell were evaluated using a BioLogic VMP-300 potentiostat. The impedance of each specimen was measured in a stagnant air atmosphere within a frequency range of 1 MHz-1 Hz and an amplitude of 50 mV. EC-Lab software was used for equivalent circuit fitting and DRT was carried out via DRT Tools developed by the Ciucci group.[3] Oxygen partial pressure (pO_2) was manipulated by mixing pure Ar and O_2 controlled by mass flow controller and the total flow rate of mixture gas was maintained at 200 sccm. For the fuel cell test condition, wet hydrogen (3% H_2O / 97% H_2) was fed into the fuel electrode and dry air was fed into the oxygen electrode. For the electrolysis test, wet hydrogen was supplied at concentrations of 3, 30, and 50% H_2O, achieved by varying the temperature of the water bubbler. The electrochemical performances of the SOCs including current density−voltage curves and impedance spectra were measured using the potentiostat (BioLogic VMP-300) in the frequency range of 1 MHz-1 Hz with an amplitude of 10 mV in both SOFC and SOEC modes. In addition, the reversibility and stability of SOCs were also evaluated.

Table S1. Crystallographic data and Rietveld refinement results for $Dy_{0.08}Y_{0.04}Bi_{0.88}O_{1.5}$ via powder XRD data: atomic coordinates, site occupancies, isotropic displacement parameters and reliability factors at room temperature.

Crystal System	Cubic
Space Group	F m -3 m (no. 225)
Lattice Parameter, Volume, Z	a = 5.5326 (1) Å, V = 169.36 (1) $Å^3$, $Z = 1$

Atoms	x	y	z	Wyckoff	Occupancy	U_{iso}
Bi1	0.0000	0.0000	0.000	*4a*	0.880	0.0359 (1)
Dy1	0.0000	0.000	0.000	*4a*	0.080	0.0359 (1)
Y1	0.0000	0.000	0.000	*4a*	0.040	0.0359 (1)
O1	0.2500	0.250	0.250	*8c*	0.243	0.0321 (1)
O2	0.3343 (1)	0.3343 (1)	0.3343 (1)	*32f*	0.127	0.1322 (1)

* $R_p = 0.079$, $R_{wp} = 0.100$, $R_{exp} = 0.059$, $R(F^2) = 0.098$, $\chi^2 = 2.924$

Table S2. Elementary ORR processes and corresponding reaction orders.[4-9]

Elementary Reactions		**Reaction Order (*m*)**	**References**
Dissociative Adsorption	$O_{2(g)} \leftrightarrow 2O_{ad}$	1	[5-8]
Charge Transfer	$O_{ad} + e' \leftrightarrow O_{ad}^{-}$	3/8	[4,5,9]
Surface Diffusion	$O_{ad}^{-} \leftrightarrow O_{TPB}^{-}$	1/4	[4,5,9]
Charge Transfer at TPBs	$O_{TPB}^{-} + e' \leftrightarrow O_{TPB}^{2-}$	1/8	[5,7,8]
O^{2-} incorporation	$O_{TPB}^{2-} + V_{o,\ electrolyte}^{\cdot\cdot} \leftrightarrow O_{o,\ electrolyte}^{X}$	0	[4-9]

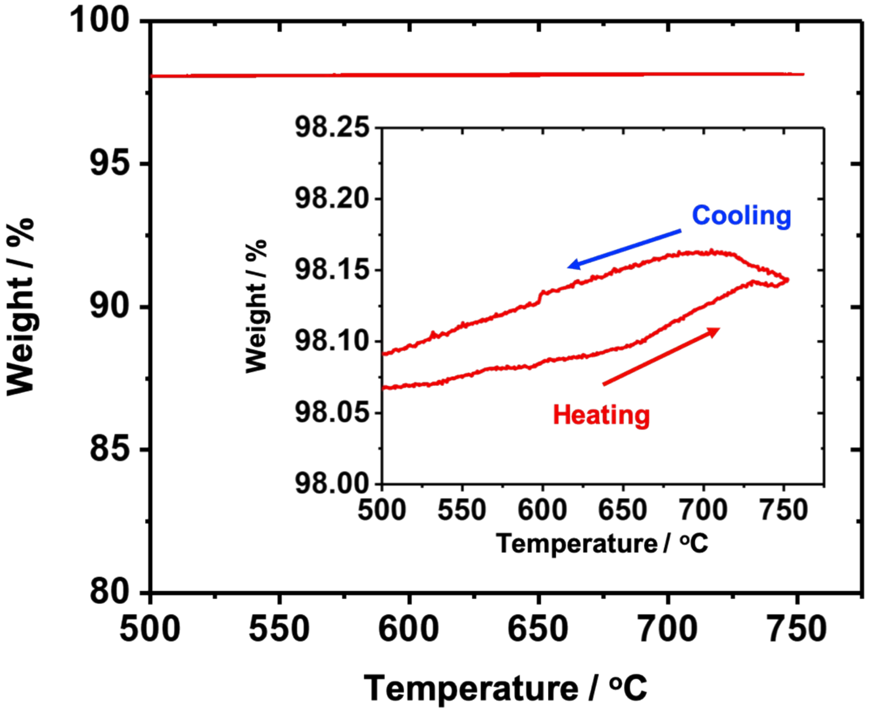

Figure S1. TGA curve of DYSB powder under air atmosphere

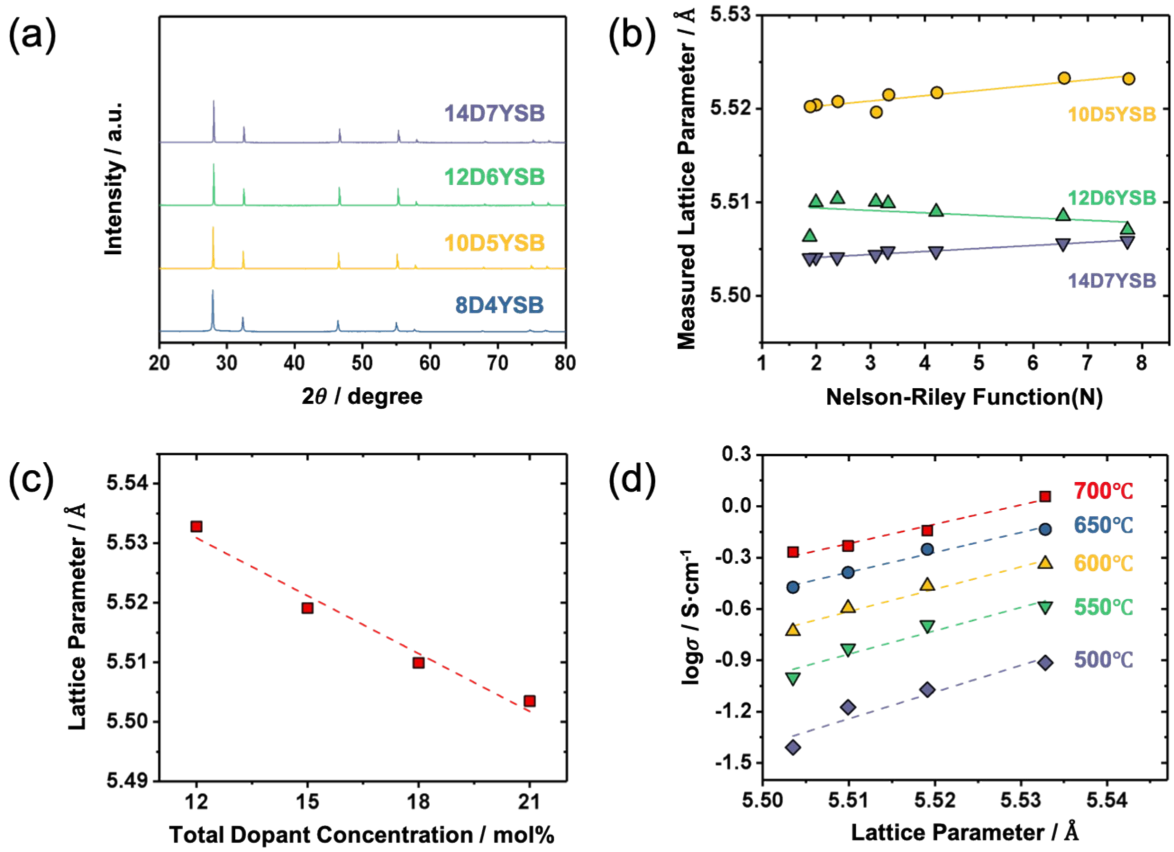

Figure S2. (a) XRD patterns of 14D7YSB, 12D6YSB, 10D5YSB and 8D4YSB. (b) Nelson-Riley extrapolation plots for DYSB powders. (c) Lattice parameters as a function of total dopant concentration and (d) total conductivity from 700 to 500 ^{o}C as a function of the lattice parameter of the DYSBs with a 2:1 dopant ratio.

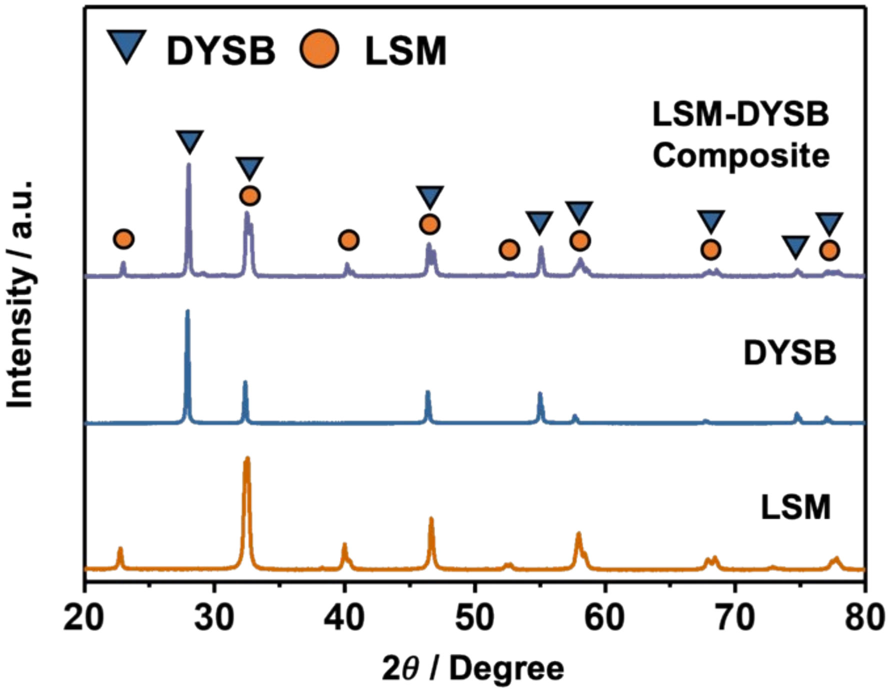

Figure S3. X-ray diffraction patterns of LSM-DYSB composite after heat-treatment at 800 oC for 5 h compared to pure DYSB and LSM powders

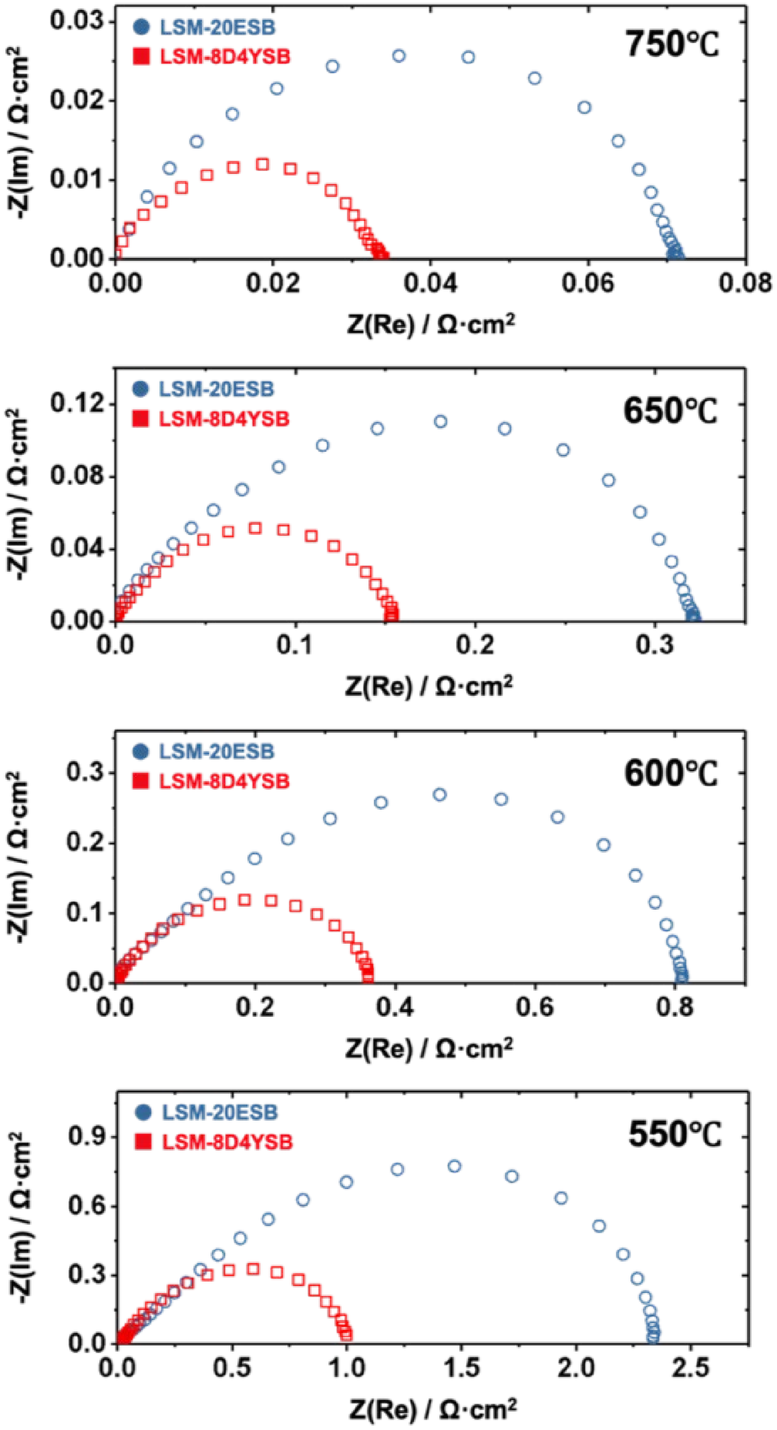

Figure S4. Nyquist plots for electrochemical impedance spectra of LSM-DYSB(red squares) and LSM-ESB(blue circles) composite cathodes on both sides of YSZ, measured under open circuit conditions from 550 to 750 °C. Nyquist plots at 700 °C are shown in Figure 2a

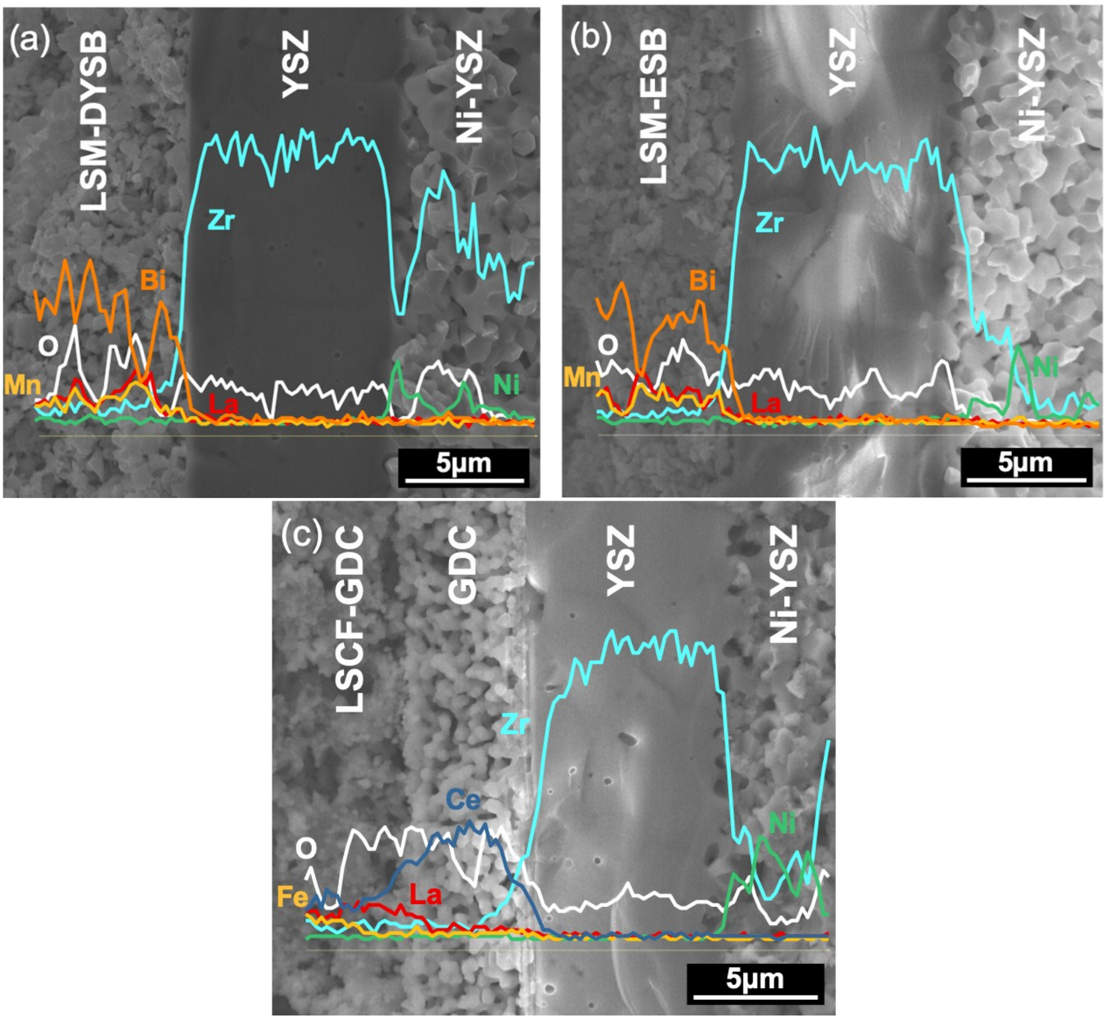

Figure S5. Cross-sectional SEM image and EDS line-scan profile of the (a) LSM-DYSB, (b) LSM-ESB, and (c) LSCF-GDC cells

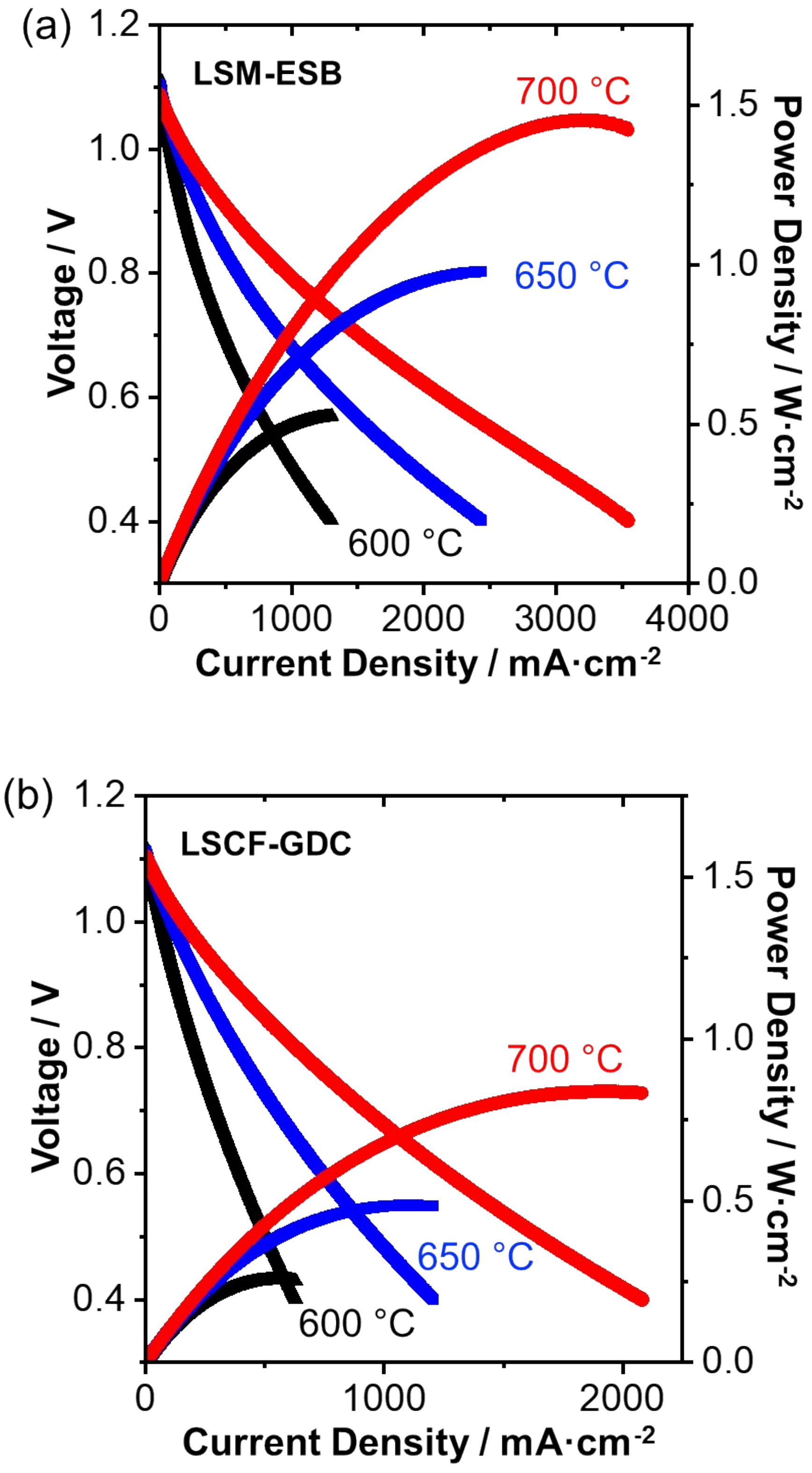

Figure S6. I-V and I-P plots of the (a) LSM-ESB and (b) LSCF-GDC cells at a temperature range from 600 to 700 °C.

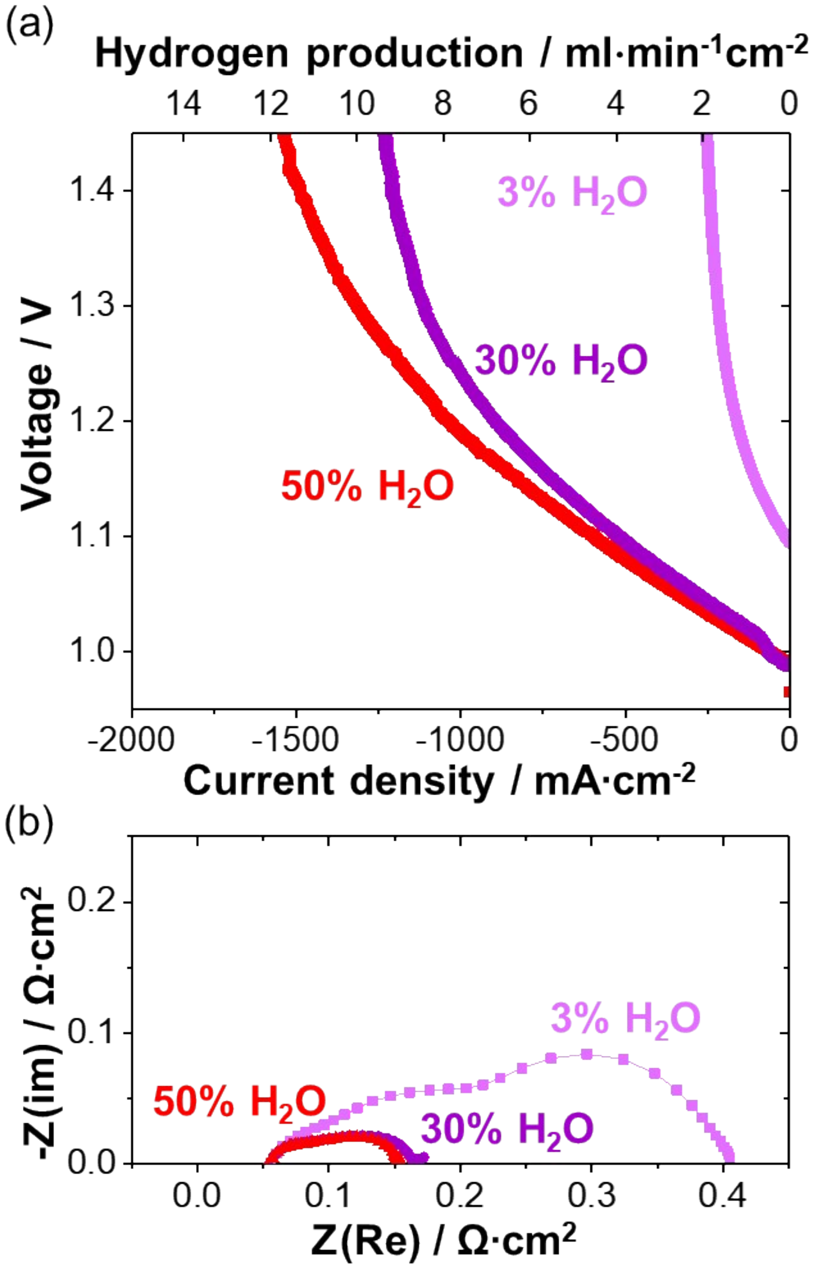

Figure S7. (a) I–V curves corresponding to H_2 production, showing the equivalent H_2 production assuming 100% Faradaic efficiency and (b) Nyquist plot in terms of electrolysis for the LSM-DYSB single cell measured at 700 °C as a function of the steam-to-hydrogen ratio (H_2O/H_2 = 50/50, 30/70, and 3/97)

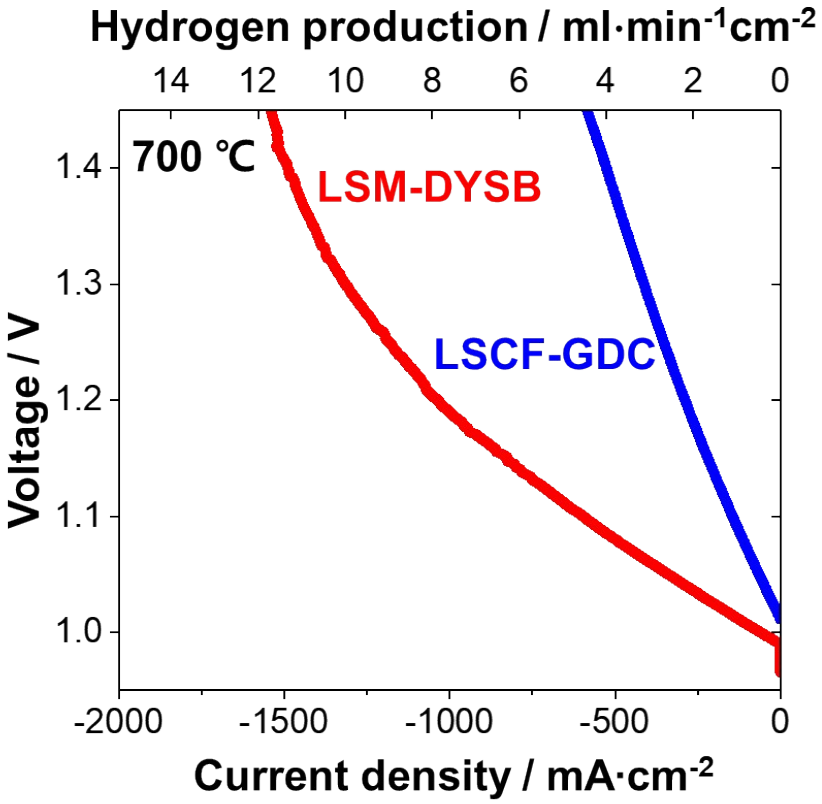

Figure S8. I–V curves comparison between LSM-DYSB and LSCF-GDC electrode corresponding H_2 production amount, showing the equivalent H_2 production assuming 100% Faradaic efficiency.

Supporting References

1. B. H. Toby, *Journal of Applied Crystallography*, 2001, **34**, 210-213.
2. S. Hull, S. T. Norberg, M. G. Tucker, S. G. Eriksson, C. E. Mohn and S. Stolen, *Dalton Trans*, 2009, 8737-8745.
3. T. H. Wan, M. Saccoccio, C. Chen and F. Ciucci, *Electrochimica Acta*, 2015, **184**, 483-499.
4. J.-D. Kim, G.-D. Kim, J.-W. Moon, Y.-i. Park, W.-H. Lee, K. Kobayashi, M. Nagai and C.-E. Kim, *Solid State Ionics*, 2001, **143**, 379-389.
5. Z. Gao, X. Liu, B. Bergman and Z. Zhao, *Journal of Power Sources*, 2011, **196**, 9195-9203.
6. S. Mulmi and V. Thangadurai, *Chem Commun*, 2019, **55**, 3713-3716.
7. L.-P. Sun, Q. Li, H. Zhao, J.-H. Hao, L.-H. Huo, G. Pang, Z. Shi and S. Feng, *International Journal of Hydrogen Energy*, 2012, **37**, 11955-11962.
8. H. Li, L.-P. Sun, Q. Li, T. Xia, H. Zhao, L.-H. Huo, J.-M. Bassat, A. Rougier, S. Fourcade and J.-C. Grenier, *International Journal of Hydrogen Energy*, 2015, **40**, 12761-12769.
9. L. Navarrete, C. Solís and J. M. Serra, *Journal of Materials Chemistry A*, 2015, **3**, 16440-16444.